

pubs.acs.org/jasms Article

Nitrile Imines as Peptide and Oligonucleotide Photo-Cross-Linkers in Gas-Phase Ions

Jiahao Wan, Marianna Nytka, Haocheng Qian, Kim Vu, Karel Lemr,* and František Tureček*



Cite This: J. Am. Soc. Mass Spectrom. 2024, 35, 344-356



ACCESS I

Metrics & More

Article Recommendations

s Supporting Information

ABSTRACT: Nitrile imines produced by photodissociation of 2,5-diaryltetrazoles undergo cross-linking reactions with amide groups in peptide-tetrazole (*tet*-peptide) conjugates and a *tet*-peptide-dinucleotide complex. Tetrazole photodissociation in gasphase ions is efficient, achieving ca. 50% conversion with 2 laser pulses at 250 nm. The formation of cross-links was detected by CID-MS³ that showed structure-significant dissociations by loss of side-chain groups and internal peptide segments. The structure and composition of cross-linking products were established by a combination of UV—vis action spectroscopy and cyclic ion mobility mass spectrometry (c-IMS). The experimental absorption bands were found to match the bands calculated for vibronic

absorption spectra of nitrile imines and cross-linked hydrazone isomers. The calculated collision cross sections (CCS_{th}) for these ions were related to the matching experimental CCS_{exp} from multipass c-IMS measurements. Loss of N₂ from *tet*-peptide conjugates was calculated to be a mildly endothermic reaction with $\Delta H_0 = 80$ kJ mol⁻¹ in the gas phase. The excess energy in the photolytically formed nitrile imine is thought to drive endothermic proton transfer, followed by exothermic cyclization to a sterically accessible peptide amide group. The exothermic nitrile imine reaction with peptide amides is promoted by proton transfer and may involve an initial [3 + 2] cycloaddition followed by cleavage of the oxadiazole intermediate. Nucleophilic groups, such as cysteine thiol, did not compete with the amide cyclization. Nitrile imine cross-linking to 2'-deoxycytidylguanosine was found to be >80% efficient and highly specific in targeting guanine. The further potential for exploring nitrile-imine cross-linking for biomolecular structure analysis is discussed.

■ INTRODUCTION

Photochemical cross-linking is an established method for structure elucidation of protein—protein and protein—nucleic acid complexes. Cross-linking relies on highly reactive intermediates that are transiently produced by photolysis of a stable precursor group (Tag), which is introduced into one component (Probe) of the complex (Scheme 1). Upon formation, the reactive group (R) undergoes rapid insertion into the sterically accessible X-H bonds in the target component (X = C, N, O), thus forming a covalent bond via a bridging group (L) and converting the complex into a molecule.

The choice of reactive groups has been limited by the requirement that the precursor is stable and can be incorporated into the complex in a site-specific manner. Carbenes^{4,5} and benzophenone excited states⁶ have been the most frequently used cross-linkers in condensed-phase applications. Cross-links can be detected by mass analysis, such as gel electrophoresis or mass spectrometry. For protein cross-linking, enzymatic digestion followed by peptide analysis by tandem mass spectrometry can be used to identify the cross-links and thus assign the contact sites in the complex.¹

We have introduced photochemical cross-linking in gasphase peptide—peptide, $^{7-12}$ peptide—nucleotide, 13 and peptide—ligand complexes, 14 as recently reviewed. 15 This has relied on carbene intermediates that were generated by UV—vis photodissociation (UVPD) of diazirine-tagged peptides or ligands. 9 Diazirine photodissociation is readily monitored by mass change in the gas-phase complex ion by N_2 elimination. Cross-links are analyzed by CID-MS 3 sequencing that allows one to identify the amino acid residues that were targeted by the carbene. 7 This scheme is fundamentally different from other methods of gas-phase covalent bond formation, such as nonselective photodissociation of small peptide complexes at 157 nm 16 or gas-phase anion—cation reactions of active esters with peptide N-terminus. 17,18 Photoexcitation at 157 nm is inherently nonselective because it does not target a particular

Received: November 1, 2023
Revised: January 3, 2024
Accepted: January 8, 2024
Published: January 22, 2024





Scheme 1. Photodissociative Cross-Linking

Scheme 2. Formation of Nitrile Imines from Tetrazoles and [3 + 2] Addition to Dipolarophiles

Scheme 3. Nitrile Imine Thermochemistry

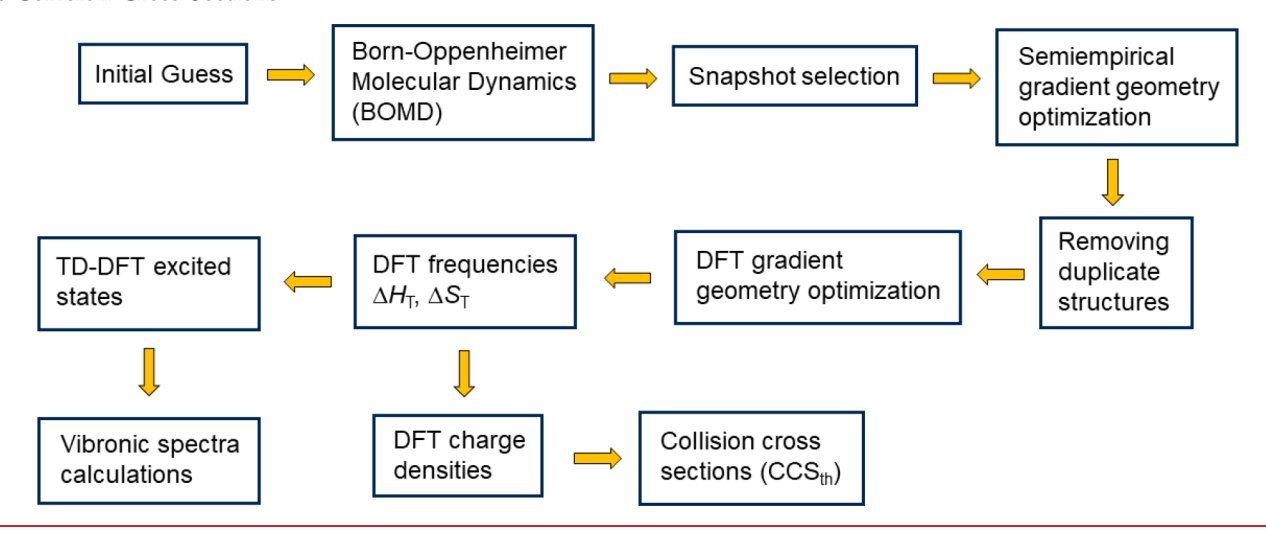
chromophore, and thus cannot be used for structure analysis of the complex. Ion—ion reactions do not address noncovalent complexes, whereas the interaction between the gas-phase reagents is dominated by strong ion—ion attractive interactions. While carbene-based cross-linking can be considered a general method of wide applicability, it also has inherent limitations. One of those is the very low extinction coefficient for the electronic excitation in the diazirine ring. This involves the dipole forbidden $\pi_{xy} \rightarrow \pi_z$ transition 19,20 that has a very low oscillator strength, which adversely affects the photodissociation conversion. Another drawback is the overall indiscriminate carbene reactivity that can attack any proximate X—H bond in the target moiety, which complicates product analysis. An alternative method of producing carbenes by CID of diazomalonate complexes has also been reported.

We now report another, rather unexpected, photochemical reaction that we apply to achieve efficient intramolecular cross-linking in peptides and intermolecular cross-linking in peptide—nucleotide complexes. The new reaction is based on nitrile imines. Nitrile imines are reactive intermediates that are known to undergo [3 + 2] cycloadditions²² to enones, alkylidene malonates, and a broad range of other dipolar-ophiles, that have been used in the synthesis of various five-membered heterocyclic systems (Scheme 2).^{23–28} As reactive intermediates, nitrile imines are readily accessible by photolysis or thermolysis of tetrazoles, by base-induced elimination from hydrazonyl halides, and by other methods.²⁹ 2,5-Diary-ltetrazole carboxylates have been used by Song et al. to

conjugate the tetrazole group to the lysine ε -amino group in peptides for further modifications by [3+2] cycloaddition with dipolarophiles. Despite the broad range of dipolarophiles used for reactions with nitrile imines, there has been a paucity of reports of reactions with functional groups pertinent to biomolecules, such as amide groups in proteins and purine and pyrimidine heterocycles in nucleic acids. Chlorinated nitrile imines have been reported to undergo [3+2] cycloaddition to enamides, but addition to an inactivated amide group has not been reported. The electronic properties of nitrile imines have been studied by Wentrup and coworkers. 31,32

The basic thermochemistry of nitrile imine generation is shown in Scheme 3 for a 2,5-diaryltetrazolecarboxamide (tet) conjugate with the pentapeptide Gly-Ala-Ala-Ala-Lys (GAAA-(tet)K + H)⁺, based on density functional theory (DFT) calculations. The calculated reaction enthalpy indicates that photodissociation at 250 nm, providing photons with 4.96 eV (479 kJ mol⁻¹) energy, is more than sufficient to break the tetrazole ring. As opposed to reactions in the condensed phase, the energy excess in the nitrile imine formation, $\Delta H_{\rm exc} \leq 479-80=399$ kJ mol⁻¹, is temporarily stored in the gas-phase ion because of slow collisional cooling^{33,34} and can be used to drive further reactions with proximate functional groups. Here, we report nitrile-imine cross-linking reactions with several peptides tagged with 2,5-diaryltetrazole. We wish to show that nitrile-imine-based reactions have the potential to be

Scheme 4. Workflow of BOMD and Density Functional Theory Calculations of Structures, Excited States, Vibronic Spectra, and Collision Cross Sections



developed into a universal method for cross-linking in biomolecular ions.

■ EXPERIMENTAL SECTION

Materials and Methods. The tet-peptide conjugates, in which the 2,5-diaryltetrazole group was attached as a carboxamide to the lysine ε -amine, were prepared by standard methods of peptide synthesis, and their sequences were confirmed by tandem mass spectrometry with accurate mass measurements (Tables S1-S4). The general procedure is described in detail in the Supporting Information. UV-vis photodissociation tandem mass spectrometry (UVPD-MS²) was performed on a Bruker amaZon ion trap mass spectrometer that was furnished with windows and focusing optics allowing the beam from an NL301G (Altos Photonics, Bozeman, MT) Nd:YAG laser to be focused into the ion trap.³⁵ The laser-ion trap mass spectrometer system was described in detail previously.³⁶ Following the previous report by Blanksby, Trevitt, and coauthors on the photodissociation of 2,5-diaryltetrazoles,³⁷ the excitation wavelength was tuned to 250 nm. Accurate mass measurements were performed on an Orbitrap Ascend Tribrid instrument (ThermoFisher, San Jose, CA) at a 100 000 resolving power. Ion mobility measurements were carried out on a SELECT SERIES cyclic ion mobility spectrometer (c-IMS) (Waters Corp., Wilmslow, UK)³⁸ with direct infusion into a normal flow electrospray ion source at a flow rate of 5 μ L/min. Each sample and calibrant were measured six times in a positive mode. Typically, ion mobility separation over five cycles was used at the total ion path of 490 cm. Details of all measurement parameters and calibration for collision cross section (CCS) calculations are given in Tables S5 and S6 and in Figure S1.

Calculations. Ion structures were obtained by a multistep procedure shown in Scheme 4. Briefly, conformers were generated by Born–Oppenheimer molecular dynamics (BOMD) calculations of 20 ps trajectories with 1 fs steps that were performed by PM6-D3H4.³⁹ These calculations were run under the high-level Cuby4 platform⁴⁰ with the Berendsen bath at 510 K.⁴¹ PM6 calculations were run under MOPAC.⁴² It should be noted that because both electron and nuclear motions are treated explicitly by BOMD, the proton positions are not fixed and can move in the course of the trajectory

calculations. Two hundred snapshots of each trajectory were taken at regular intervals and fully gradient-optimized with PM6-D3H4. The resulting structures were compacted by removing duplicates and submitted to gradient geometry optimization with B3LYP⁴³ that was augmented by empirical dispersion terms⁴⁴ with Becke–Johnson damping (GD3-BJ).⁴⁵ B3LYP-GD3-BJ was also used to calculate harmonic frequencies. Additional sets of optimized geometries were obtained by M06-2X calculations 46 with the 6-31+G(d,p) basis set that were also used for single-point energy calculations with M06-2X/6-311++G(2d,p). Charge distributions were calculated according to Merz, Singh, and Kollman (MK). 47,48 Collision cross sections were calculated by the modified ion trajectory method (MobCal_{MPI})^{49,50} using the MK charge densities. Excited states were calculated by time-dependent density functional theory⁵¹ using M06-2X/6-31+G(d,p). Typically, 15-20 excited states were considered. Vibronic absorption spectra were calculated for electronic excitations from 300 Wigner configurations 52,53 that were generated from B3LYP vibrational frequencies and sorted out by their Boltzmann factors. These calculations were run using the NewtonX software.5

■ RESULTS AND DISCUSSION

Photodissociation of Tetrazole-Peptide Conjugates.

The tet-peptide conjugates were protonated by electrospray ionization, selected by mass, and subjected to laser photodissociation. In addition, sodiated ions, (tet-peptide-COONa + Na)⁺, were generated from solutions containing sodium acetate and used for UVPD. Photodissociation of all tet-peptide ions at 250 nm was efficient, achieving up to 50% conversions after just two 2 mJ laser pulses. This is illustrated with the $(AAFA(tet)K + H)^+$ ions (m/z 755) that were generated by electrospray and submitted to photodissociation (Figure 1a). Similar to previous studies in solution, 22 UVPD-MS2 primarily resulted in N2 loss, forming the transient nitrile imine intermediate at m/z 727. Loss of N₂ upon photodissociation of gas-phase 2,5-diaryltetrazole ions has been reported by Blanksby, Trevitt, and coauthors who measured the extinction coefficients as $\varepsilon \cong 2 \times 10^4 \text{ L mol}^{-1} \text{ cm}^{-1}$ at $\lambda_{\text{max}} = 255 \text{ nm.}^{37}$ Our UVPD efficiencies at 250 nm for tet-tagged peptides were consistent with the previous measurements. In addition to loss

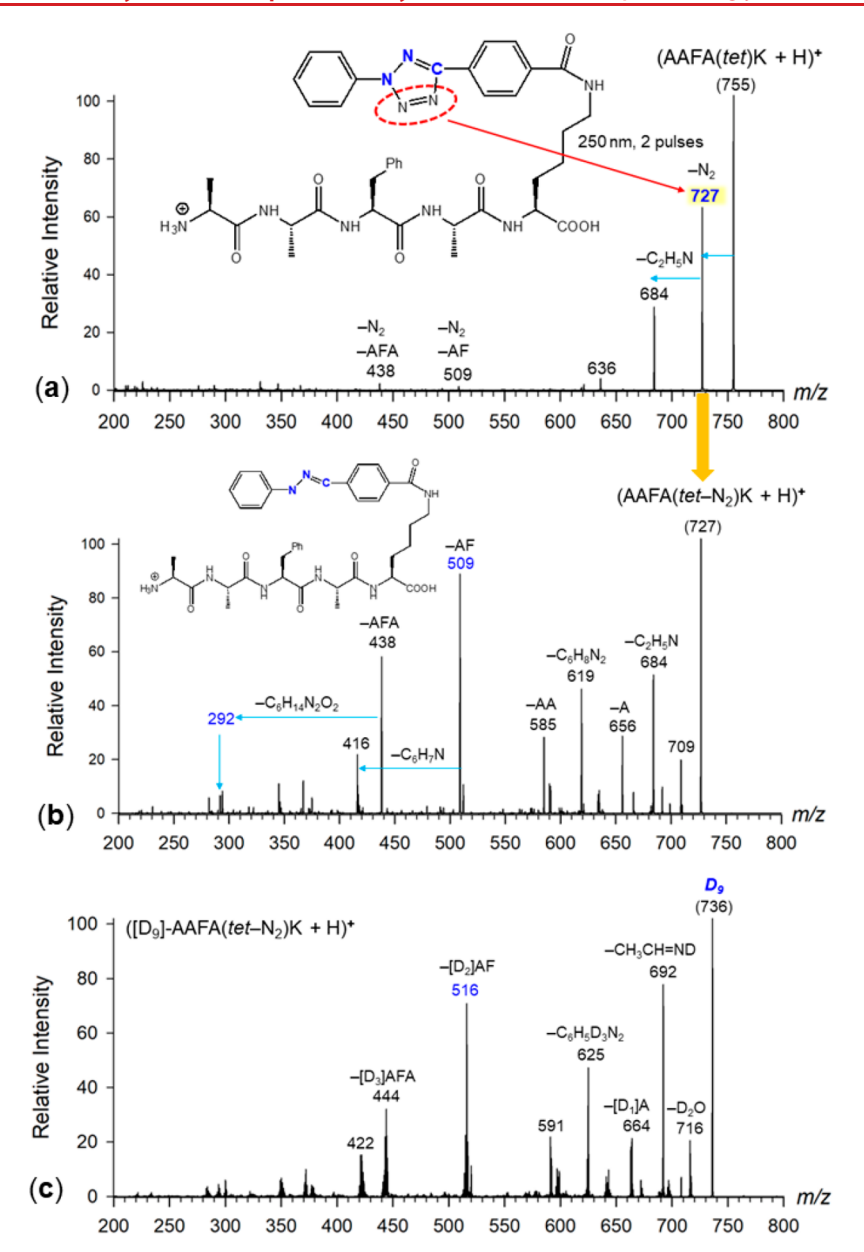


Figure 1. (a) UVPD-MS² spectrum of (AAFA(tet)K + H)⁺ (m/z 755). (b) CID-MS³ spectrum of (AAFA(tet-N₂)K + H)⁺ (m/z 727) from (a). (c) CID-MS³ spectrum of ([D₉]-AAFA(tet-N₂)K + H)⁺ (m/z 736). For ion assignment by accurate mass measurements, see Table S1.

of N_2 , the UVPD-MS² spectrum showed consecutive loss of C_2H_5N (m/z 684), which is an atypical peptide ion dissociation. Loss of N_2 was also the main dissociation of (AAFA(tet)K + H)⁺ that was triggered by collision-induced dissociation (CID) that allowed us to measure accurate m/z and assign elemental composition to the ions (Table S1).

CID-MS³ of Nitrile Imine Intermediates. Further analysis of the (AAFA(tet-N₂)K + H)⁺ ions was carried out by UVPD-CID-MS³ (Figure 1b,c). The spectrum showed internal sequence fragment ions by loss of Ala-Phe and Ala-Phe-Ala neutral internal residues, which are typically not produced from linear peptide chains,⁵⁵ while being indicative of cyclic peptide structures.⁵⁶ Accordingly, the reference CID spectrum of the (AAFA(tet)K+H)⁺ ion showed a series of standard C-terminal y_1 – y_3 fragment ions but no internal losses (Figure S2). Fragment ions of the y_n type were also present in the UVPD-CID-MS³ (Figure 1b) and CID-CID-MS³ spectra of (AAFA(tet-N₂)K + H)⁺ (Figure S3). However, the pattern

of relative intensities of these sequence ions from (AAFA(tet- N_2)K + H)⁺ markedly differed from those in the Figure S2 reference spectrum, indicating that they may be formed by loss of internal neutral peptide residues instead. Another indication of cross-linking was by loss of neutral lysine (C₆H₁₄N₂O₂) from the m/z 438 ion (m/z 292, Figures 1b and S3), which was incompatible with a y_2 structure, but could be accommodated if the N-terminal Ala was covalently linked to the nitrile imine moiety. In addition to internal fragments, the Figure 1b spectrum also showed losses of C₂H₅N from the Ala N-terminus and $C_6H_8N_2$ from the nitrile imine group. The CID-MS³ spectrum of $(AAFA(tet-N_2)K + H)^+$ ions that were generated by collision-induced loss of N2 from the tetrazole ring was entirely similar to that of ions produced by photodissociation (Figure S3). The assignment of the neutral losses as being internal peptide fragments was corroborated by the UVPD-CID-MS³ spectrum of $(AGFA(tet-N_2)K + H)^+$ that showed a loss of Gly-Phe and not Phe-Ala (Figure S4). All of these dissociations indicated that the nitrile imine group produced by photodissociation or CID was engaged in a ring-forming reaction with the peptide chain. The neutral fragments were identified by deuterium labeling. The ([D₉]-AAFA(tet-N₂)K + H)⁺ ion (m/z 736, Figure 1c), generated from ([D₉]-AAFA(tet)K + H)⁺ after exhaustive H/D exchange, showed loss of C₂H₄DN and C₆H₅D₃N₂ that pointed to acetaldimine and phenyl hydrazine for the respective neutral molecules.

We have further investigated the effect on nitrile imine formation and dissociations of modifying the C-terminus and N-terminal amino acid residues in the peptide-tet conjugates. Blocking the carboxyl terminus as a methyl ester in (AAFA(tet- N_2)K-OCH₃ + H)⁺ gave CID-MS³ that was analogous to that of (AAFA(tet-N₂)K + H)+, showing loss of acetaldimine, phenylhydrazine, and internal Ala-Phe and Ala-Phe-Ala fragments (Figure S5). Modifications of the N-terminal residues, such as in $(GAAA(tet)K + H)^+$, (CAAA(tet)K +H)⁺, (NAAA(tet)K + H)⁺, and (QAAA(tet)K + H)⁺, did not affect UVPD, resulting in an efficient loss of N2 and nitrile imine formation in each case (Figure S6). Similarly, placing the tet-tagged lysine at the N-terminus as in $((tet)KAAAG + H)^+$ resulted in an efficient N₂ loss upon UVPD (Figure S7a). The CID-MS³ dissociations showed variations in the relative intensities of fragment ions, which, however, followed the general features displayed by (AAFA(tet-N₂)K + H)⁺ (Figure 1b). For example, CID-MS³ of the m/z 637 ion from (GAAA(tet-N₂)K + H)⁺ showed prominent loss of CH₂= NH from the Gly N-terminus in addition to elimination of phenylhydrazine (Figure S8a). Internal fragments by loss of Ala-Ala and Ala-Ala-Ala at m/z 495 and 424, respectively, attested to a ring structure formed by nitrile imine crosslinking. The ion assignments were corroborated by accurate mass measurements (Table S2). CID-MS³ of (CAAA(tet-N₂)K + H)+ (Figure S8b) showed a very prominent loss of phenyl hydrazine in addition to the loss of C₂H₅NS from the Nterminal cysteine, represented as a HSCH₂CH=NH imine fragment, and internal fragments by loss of Ala-Ala and Ala-Ala-Ala that were accompanied by loss of H₂S. These dissociations indicated that the cysteine thiol group was not engaged in the ring-forming cross-linking. Note that nucleophilic additions to nitrile imines have been observed in solution, ^{22,23} and hence the lack of reactivity for the cysteine thiol was remarkable. CID-MS³ in the presence of side chain amide groups, such as in (NAAA(tet-N2)K + H)+ and (QAAA(tet-N2)K + H)+, resulted in an enhanced loss of ammonia. However, dissociations leading to the loss of the Nterminal group, HN=CH-CH2CONH2 and HN=CH-CH₂CH₂CONH₂ from asparagine and glutamine, respectively, were observed, as were losses of internal Ala-Ala and Ala-Ala-Ala fragments (Figure S8c,d). These common dissociations of the N-terminal aldimine fragments, HN=CH(R), pointed to cross-linking to the nitrile imine by an amide group within the peptide sequence. Some level of participation by the side-chain amide groups in Asn and Gln could not be completely excluded and may be the reason for the enhanced loss of ammonia from these peptide conjugates.

CID-MS³ of the inverted sequence ion, $((tet-N_2)KAAAG + H)^+$, showed a major loss of water and internal fragments by loss of Gly, Ala, Ala-Gly, Ala-Ala, and Ala-Ala-Ala (Figure S7b). Fragment ions of the b_n type, which are characteristic of glycine C-terminated N-linked conjugates, ⁵⁷ were absent in the CID-MS³ spectrum of $((tet-N_2)KAAAG + H)^+$, indicating nearly complete cyclization involving the glycine residue. In

particular, the loss of Gly as HNCH₂CO (57 Da) and Ala-Gly (128 Da) was indicative of a carboxyl linkage to the nitrile imine.

We further investigated the effect of the charging ion using sodiated conjugates, $(AAFA(tet-N_2)K-COONa + Na)^+$, m/z 771 (Figure S9a), and $(GAAA(tet-N_2)K-COONa + Na)^+$, m/z 681 (Figure S9b), that were produced by UVPD at 250 nm of the sodiated precursor ions. In both cases, the CID-MS³ spectra showed a series of y_1-y_3 sequence ions that were identified by accurate mass measurements (Tables S3 and S4). In contrast to the above-described protonated ions, no internal fragments were found for the sodiated ions that would indicate cross-linking. This pointed to the possible role of the charging proton in promoting the peptide reactions with the nitrile imine group.

Structures and UV-Vis Action Spectra of Nitrile-**Imine Cross-Links.** The fundamental question regarding the observed cyclizations in protonated ions was whether they occurred upon the photochemical nitrile imine formation or were promoted by subsequent collisional activation of isolated stable nitrile imine ions. To answer this question, we used action spectroscopy to obtain the UV-vis spectra of the $(AAFA(tet-N_2)K + H)^+$ and $(GAAA(tet-N_2)K + H)^+$ ions. The spectra were obtained in the CID-UVPD mode where the nitrile imine ions used for the action spectra measurements were generated by CID-MS² from the tetrazole conjugates. Because CID in the ion trap is performed in a mass-resonant mode, the resulting (peptide($tet-N_2$)+ H)⁺ ions are not further activated. The action spectrum of $(GAAA(tet-N_2)K + H)^+$, which has only a nitrile-imine related chromophore absorbing in the 210-700 nm region, is representative (Figure 2a).

The action spectrum was monitored for the m/z 608 (loss of CH₂=NH, major fragment ion), m/z 495 (loss of Ala-Ala), m/z 424 (loss of Ala-Ala-Ala), and m/z 367 (loss of Gly-Ala-Ala-Ala) photofragment ion channels. The spectrum showed a

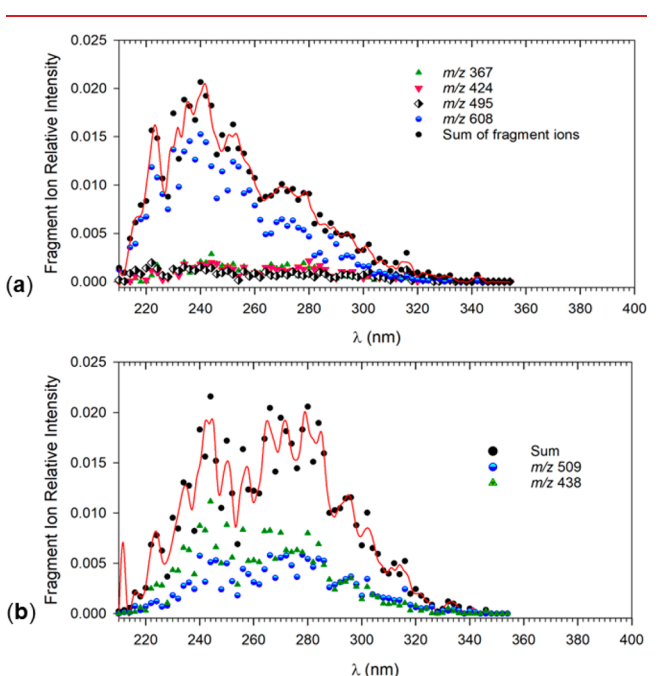


Figure 2. UVPD action spectra of (a) $(GAAA(tet-N_2)K + H)^+$ and (b) $(AAFA(tet-N_2)K + H)^+$. The red outline is a fit to the sum of photofragment ion intensities.

composite band with maxima at 220, 240, and 250 nm, and another weaker broad band at 270 nm. These maxima appeared in at least two photofragment ion channels, namely, m/z 608 and m/z 495, which were indicative of cross-linked structures.

No absorption was detected above 350 nm. The action spectrum of $(AAFA(tet-N_2)K + H)^+$ (Figure 2b) was monitored for the m/z 509 (loss of Ala-Phe) and m/z 439 (loss of Ala-Phe-Ala) channels. The spectrum showed a broad band consisting of three maxima at 240, 265–280, and 290–320 nm. The third band was visible in the m/z 509 ion channel. No absorption was observed above 350 nm.

To interpret the spectra and assign the absorption bands, we carried out extensive BOMD and density functional theory (DFT) calculations of ion structures and excited electronic states for $(GAAA(tet-N_2)K + H)^+$ and $(AAFA(tet-N_2)K + H)^+$. The initial guesses in these calculations were nitrile imine protomers and conformers, as well as cyclized structures involving functional groups that can potentially give rise to the major fragment ions in the CID-MS³ spectra. These features involved a free neutral or protonated Gly CH2NH2 group to account for the loss of CH₂=NH, and a retained phenyl-N-N segment for the loss of phenylhydrazine. The lowest-energy structures of each type are shown in Figure 3. For several (GAAA(tet-N₂)K + H)⁺ isomers, we also calculated vibronic absorption spectra at 350 K that included excitations from 300 configurations representing the vibrational states of the ions. The low-energy nitrile imines (G1 and G2) showed vibronic spectra that strongly depended on the ion conformation. The lowest-energy conformer G1 (Figure 3) showed a very weak transition to the first excited state at 438 nm (Figure 4a). The main transitions at 272, 269, and 246 nm gave rise to the compact band in the vibronic spectrum with a maximum at 270 nm. Vibronic broadening of the 269 and 272 nm bands then resulted in a band tail extending to 360 nm (Figure 4a). The other low-energy conformer (G2, 13 kJ mol⁻¹ relative to G1, Table 1) showed a strong transition to the second excited state at 290 nm that was spread over a broad range of transitions in the thermal ion reaching beyond 400 nm (Figure 4b). Structures produced by simple proton transfer to the nitrile imine group (G3, 28 kJ mol⁻¹ relative to G1) showed a strong transition to the first excited state at 330 nm (Figure 4c) that was incompatible with the action spectrum. The lowest energy structures belonged to hydrazidines (e.g., G4, -84 kJ mol⁻¹ relative to G1) arising by nucleophilic attack at the nitrile imine by the Gly amine group. However, the vibronic spectrum of G4 showed major bands at 220 nm and an absorption profile that was incompatible with the action spectrum (Figure 4d). Oxadiazoles were another type of product that could have arisen by the formal [3 + 2] addition of the Gly amide to the nitrile imine. The lowest energy oxadiazole isomer (G5, -68 kJ mol⁻¹ relative to G1) had a vibronic spectrum that showed a strong transition at 310 nm that resulted in bands at 315 and 345 nm that, however, were absent in the action spectrum (Figure 4e).

Since, according to the calculations, the oxadiazole C–O bond in **G5** was weak ($\Delta H_{\rm rxn} = 24 \text{ kJ mol}^{-1}$), breaking it was considered to be facile. Opening of the oxadiazole ring, followed by proton transfer, formed N–C linked hydrazones that are represented as conformers **G6** and **G7** (–44 and –43 kJ mol⁻¹, respectively, relative to **G1**). The respective vibronic spectra showed bands in the 240–260 nm region (Figure 4f,g), and the position of the maxima and the shape of these bands

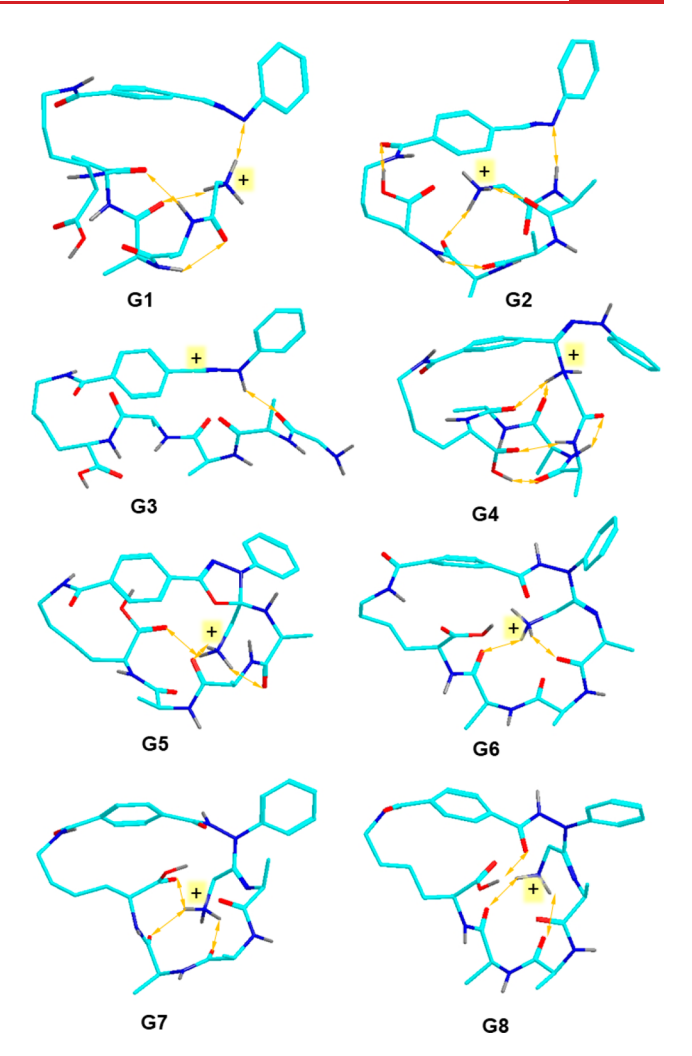


Figure 3. M06-2X/6-31+G(d,p) optimized structures of representative low-energy (GAAA(tet-N₂)K + H)⁺ ions **G1–G8**. Atom color coding is as follows: cyan = C, blue = N, red = O, gray = H. Only exchangeable hydrogens are shown to avoid clutter. Hydrogen bonds are visualized by ochre double-headed arrows.

were in good agreement with the bands in the action spectrum. Another low-energy conformer of this type (G8, Figure 3) had a vibronic spectrum (Figure 4h) that was very similar to those of G6 and G7, illustrating the general features of the diarylhydrazone chromophore. In summary, structures G1 and G6–G8 provided the best match with the action spectrum of the (GAAA(tet-N₂)K + H)⁺ ion.

Electronic excited states were also analyzed using TD-DFT calculations of several potential isomers of the (AAFA(tet- N_2) K + H)⁺ ions. Because of the larger size of these ions, we were unable to calculate vibronic spectra, and so the assignment relied on the 0 K vertical excitations only, whereas absorption profiles due to thermal band shifts and broadening were not included. The optimized structures and calculated TD-DFT transitions are shown in Figure S10. Overall, the structure assignment for (AAFA(tet- N_2)K+ H)⁺ was consistent with that discussed above for (GAAA(tet- N_2)K+ H)⁺. In particular, the lowest-energy nitrile imine conformer (F1) had a strong transition at 339 nm that was absent in the action spectrum. Protonated diarylhydrazine (F2) formed by N-terminal amine addition to the nitrile imine had strong transitions in the 210 nm region that were not present in the action spectrum.

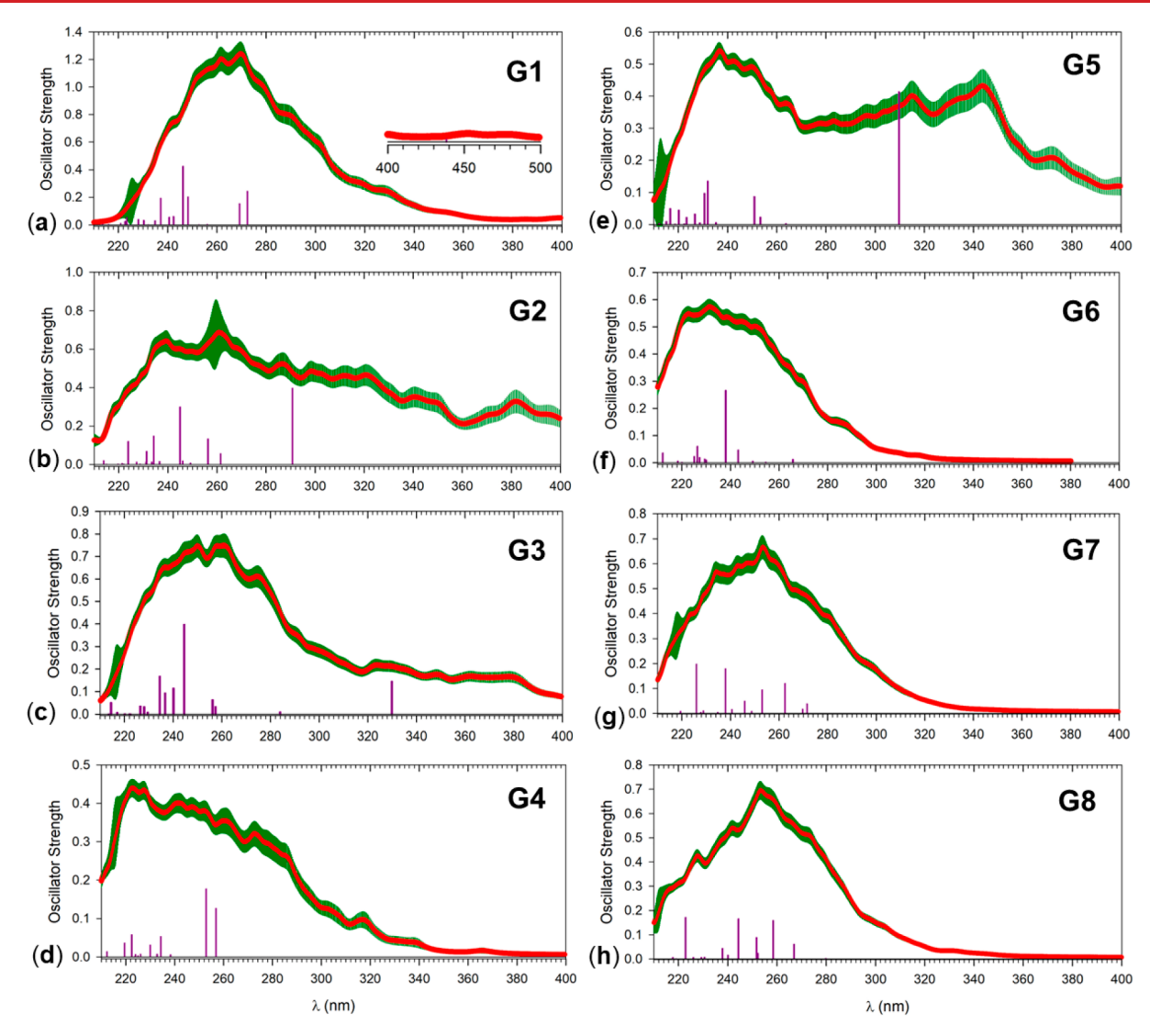


Figure 4. (a-h) M06-2X/6-31+G(d,p) vibronic spectra of $(GAAA(tet-N_2)K + H)^+$ isomers G1-G8. Vertical lines represent TD-DFT electron transitions at 0 K. For ion structures, see Figure 3.

Table 1. Calculated Relative Energies and Collision Cross Sections of $(GAAA(tet-N_2)K + H)^+$ Ions

·		
ion	relative energy ^{a,b,c}	CCS^d
G1	0 (0)	249.6 ± 1.0^{e}
G2	13 (19)	245.3 ± 1.2
G3	28 (17)	257.5 ± 1.4
G4	-84 (-65)	231.5 ± 1.0
G5	-67 (-54)	241.3 ± 0.6
G6	-43 (-33)	251.3 ± 1.4
G 7	-44 (-30)	241.5 ± 1.0
G8	-32 (-18)	242.9 ± 1.0

^aIn kJ mol⁻¹. ^bFrom M06-2X/6-311++G(2d,p) single-point energy calculations including zero-point energies and referring to 0 K. ^cRelative Gibbs energies at 310 K in parentheses. ^dIn Å². ^eStandard deviations from multiple runs (n = 10).

Oxadiazole adducts, as represented by structures **F3** and **F4**, showed strong transitions at 285 nm that were expected to be red-shifted at 310 K and would not match the action spectrum of $(AAFA(tet-N_2)K + H)^+$. A tentative match can be expected for hydrazidine **F5** where the electron transitions at 230-260 nm (Figure S10) are likely to be red-shifted in a vibronic

spectrum to form bands at 240-280 that were observed in the action spectrum of $(AAFA(tet-N_2)K + H)^+$. Note that structure **F5** was protonated in the hydrazidine group, which differed from **G6–G8** that were protonated in the *N*-terminal amine (Figure 3).

Cyclic Ion Mobility Measurements. In an effort to further characterize the ions of interest, we investigated the composition and structures of the peptide tetrazole conjugates and their cross-linked products using cyclic ion mobility spectrometry (c-IMS).³⁸ This allowed us to separate isomers by their arrival times and obtain collision cross sections (CCS_{exp}) in N_2 . The $(AAFA(tet)K + H)^+$ and (GAAA(tet)K +H)⁺ ions showed single peaks after five passes (490 cm path length) of c-IMS, indicating structurally homogeneous ions (Figure 5). The measured $CCS_{exp} = 273$ and 256 Å² for $(AAFA(tet)K + H)^+$ and $(GAAA(tet)K + H)^+$, respectively, were matched by the calculated CCSth for the lowest Gibbsenergy conformers of these ions (Figure 5). The ions of both sequences were protonated at the N-terminus regardless of the initial proton position in structures that were submitted to BOMD. The optimized structures showed globular peptide moieties that were maintained by multiple intramolecular

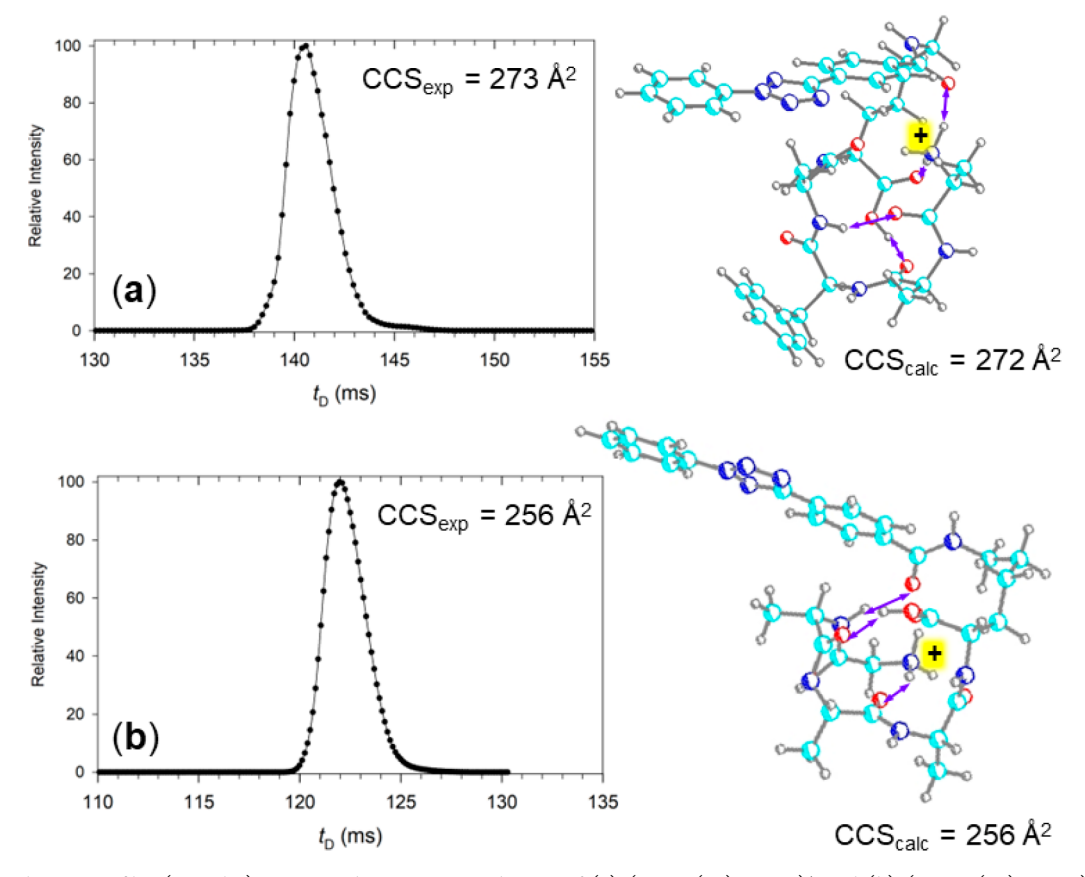


Figure 5. Arrival time profiles (5 cycles), optimized structures, and CCS of (a) $(AAFA(tet)K + H)^+$ and (b) $(GAAA(tet)K + H)^+$. Atom color coding is as in Figure 3. Hydrogen bonds are visualized by double-headed purple arrows.

hydrogen bonds. The 2,5-diaryl tetrazole moiety was positioned at the ion periphery and, with the exception of its carbonyl, was not linked by hydrogen bonds to the peptide polar groups. This indicated that the tetrazole group may be viewed as a spectator without significantly affecting the peptide ion conformation. However, the rigid structure of the 2,5-diaryl tetrazole moiety limits access of the incipient nitrile imine to amide bonds and other functional groups to be located close to the pentapeptide *N*-terminus. From the optimized structures, one can assess the minimum number of four residues that separate the tetrazole ring and the incipient nitrile imine from the nearest sterically possible cross-linking site.

In contrast to the precursor ions, the $(AAFA(tet-N_2)K + H)^+$ and $(GAAA(tet-N_2)K + H)^+$ ions generated by CID were mixtures of isomers (Figure 6). According to c-IMS, $(AAFA(tet-N_2)K + H)^+$ produced one major peak of CCS_{exp} = 268 Ų, amounting to ca. 80% of the total ion intensity.

This major peak was flanked by two minor peaks (Figure 6a). (GAAA(tet-N₂)K + H)⁺ produced two major peaks of CCS_{exp} = 246 and 254 Ų that were accompanied by two additional minor peaks (Figure 6b). The CCS_{exp} values of (GAAA(tet-N₂)K + H)⁺ were compared to those of CCS_{th} that were calculated for several structure types (G1–G8, Table 1). Nitrile imines G1 and G2 had CCS_{th} in the 246–250 Ų range that overlapped with the 246 Ų peak in Figure 6b. Considering the minor band at 270 nm in the Figure 2a action spectrum that can be attributed to a nitrile imine, the combined data indicated the presence of an unreacted nitrile imine in the mixture. Consistent with this conclusion, the CID-MS³ spectrum of (GAAA(tet-N₂)K + H)⁺ (Figure S8a)

showed a minor y_2 ion at m/z 438, which indicated loss of a Gly-Ala-Ala b_3 neutral fragment from the straight peptide chain. The CCS_{th} of the protonated nitrile imine isomer G3 (257.5 Å²) was close to that of the second major peak in the c-IMS arrival time profile. However, isomer G3 was excluded on the basis of its incompatible absorption spectrum (Figure 4c). The low-energy hydrazidine G4 had a CCS_{th} that did not match any of the experimental values and, in accordance with its nonmatching vibronic spectrum (Figure 4d), was excluded. The CCS_{th} of oxadiazole G5 was at the low end of the CCS_{exp} values; however, its vibronic spectrum (Figure 4e) did not match the action spectrum. The CCS_{th} of hydrazones G6 (251.3 Å^2) and G7 (241.5 Å^2) matched within -1.1% and -1.8%, respectively, the CCS_{exp} of the major peaks from c-IMS. In addition, another conformer of the same type (G8) had $CCS_{th} = 243 \text{ Å}^2$, which was within -1.1% of the CCS_{exp} of the major c-IMS peak. In addition to having closely related CCS, structures G6-G8 also had vibronic spectra that match the major bands in the action spectrum of $(GAAA(tet-N_2)K +$ H)+. Hence, the combination of c-IMS and UV-vis action spectroscopy provided data that upon analysis allowed us to assign probable structures to the reaction products while excluding those that showed close fits in only one type of experimental data.

The formation of cross-linked structures **G6–G8** and **F5** raised the question of the pertinent reaction mechanism(s). These structures showed the formation of a C=O bond by amide oxygen transfer to the nitrile imine carbon, and a new C-N bond to the imine nitrogen. We proposed a tentative mechanism that accounts for these changes in (GAAA(tet-N₂)

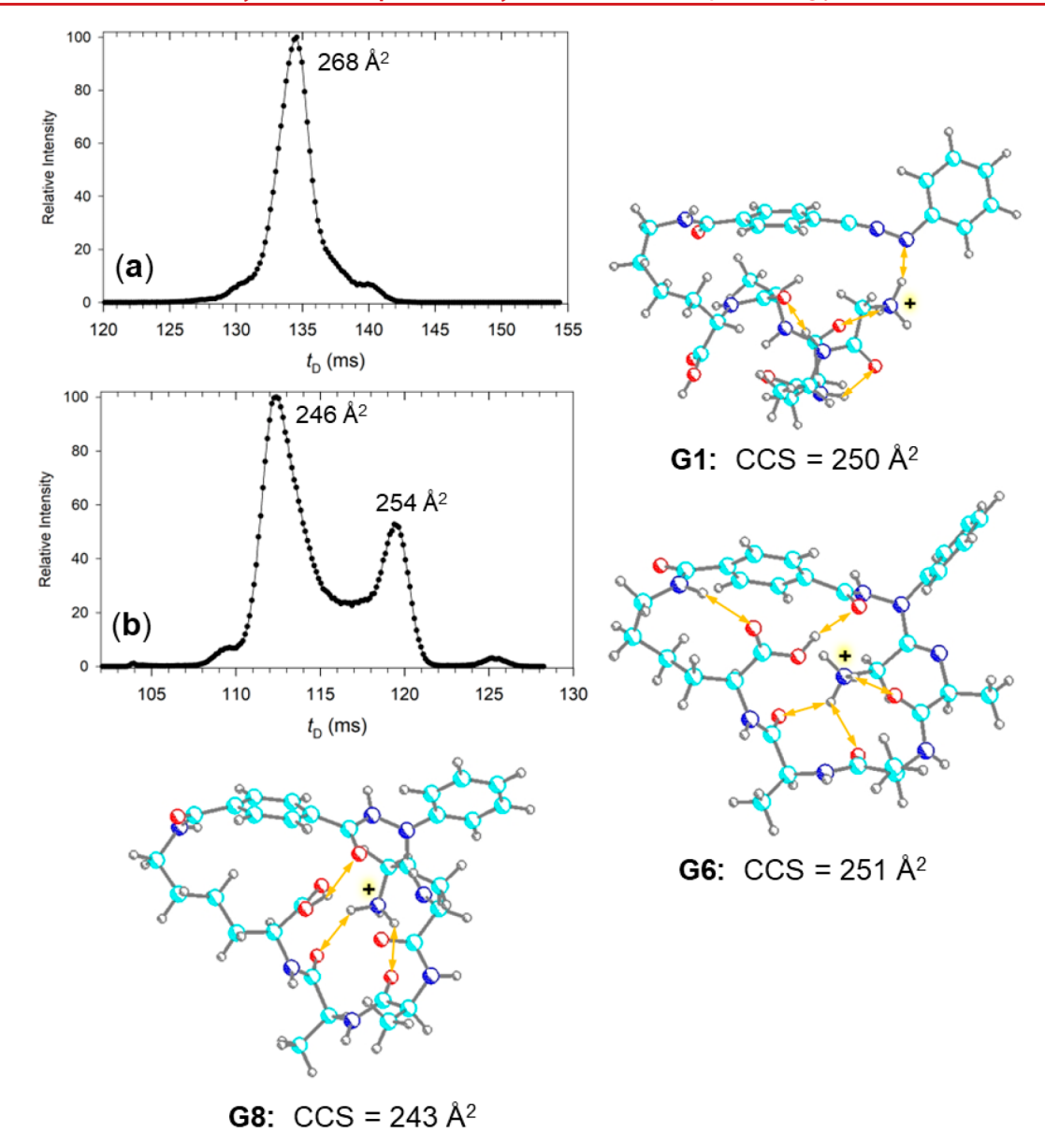


Figure 6. Arrival time distributions after five passes of (a) $(AAFA(tet-N_2)K + H)^+$ and (b) $(GAAA(tet-N_2)K + H)^+$ with experimental CCS_{exp} for the major peaks and matching calculated ion structures.

 $(K + H)^{+}$, which is shown in Scheme 5. A formal [3 + 2]addition of the Gly amide to the nitrile imine was presumed to initially form intermediate 3. This step may be facilitated by proton transfer to the nitrile imine; note that the role of catalytical initial proton transfer was corroborated by the absence of cross-linking in sodium ion adducts (Figure S9) that lacked active protons. The protonated oxapyrazoline ring in 3 presumably opened by breaking the quaternary C-O bond, forming a hydrazide (4), which in (GAAA(tet-N₂)K + H) $^+$ was finally stabilized by proton migration back to the Nterminal amine group, producing conformers 2a,2b. Structures 2a,2b were compatible with the major dissociations of $(GAAA(tet-N_2)K + H)^+$ ions upon CID that showed loss of CH₂=NH and PhNHNH₂ (Figure S8a) and analogously for the other XAAAK-tet sequences (Figure S8b-d). The final step of proton migration $(4 \rightarrow 2a,b)$ may be reversible, depending on the basicity of the pertinent nitrogen atoms and proton stabilization by hydrogen bonding. For example, the (AAFA(tet-N2)K + H)+ structure F5 was protonated in the

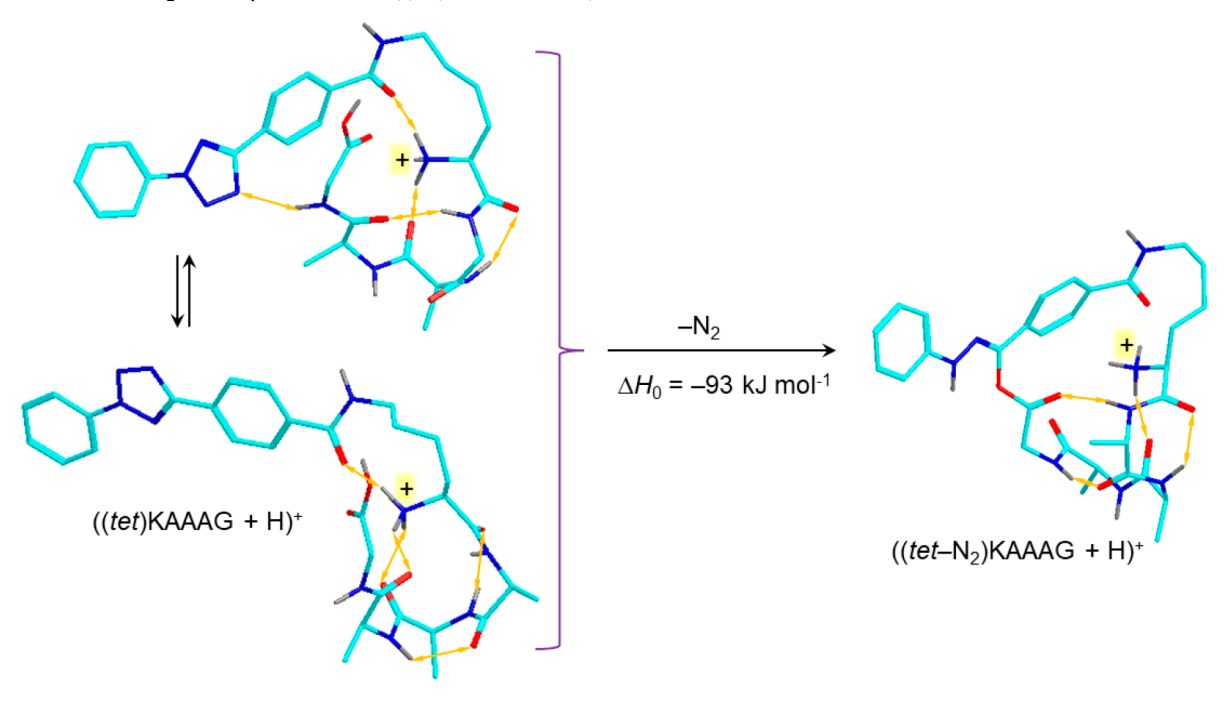
hydrazidine group (Figure S10), analogous to intermediate 4 in Scheme 5.

Cross-linking to the C-terminal residue, as in (($tet-N_2$)KAAAG + H)⁺, may involve simple nucleophilic attack by the carboxyl at the nitrile imine that is promoted by proton transfer. Scheme 6 indicates that the overall reaction from ((tet)KAAAG + H)⁺ to the cyclized (($tet-N_2$)KAAAG + H)⁺ product is substantially exothermic and thus possible following photodissociation. The conformations of the lowest-energy ((tet)KAAAG + H)⁺ precursor ions in Scheme 6 allow a facile access of the carboxyl proton and oxygen to the nitrile imine for proton transfer and ring closure. The role of the charged N-terminal NH₃ group in reversibly providing the proton has not been established and would require an extensive transition-state search to be elucidated.

Nitrile Imine Cross-Linking in a Peptide-Dinucleotide Complex. To further explore the nitrile-imine reactivity toward other functional groups, we investigated the non-covalent ion complex of dinucleotide 2'-deoxycytidylguanosine

Scheme 5. Proposed Mechanism for Nitrile Imine-Amide Cross-Linking

Scheme 6. Loss of N_2 and Cyclization in $((tet)KAAAG + H)^{+a}$



 a The reaction enthalpy is from M06-2X/6-311++G(2d,p) + ZPVE calculations and refers to 0 K. Atom color coding is as in Figure 3.

(dCG) with the GAAA(tet)K peptide. The singly protonated complex, (dCG-GAAA(tet)K + H)⁺, was produced by electrospray ionization, selected by mass (m/z 1221), and submitted to UVPD. Figure 7a shows that efficient (>50%) photodissociation was achieved in 2 laser pulses at 250 nm that triggered loss of N₂ from the tetrazole ring. CID-MS³ of the mass-selected photoproduct (m/z 1193, Figure 7b) resulted in a highly selective loss of cytosine (C, m/z 1082) and deoxycytidine (dC, m/z 984) by standard phosphoric ester elimination. S8,59 In contrast, no loss of guanosine was observed, as evidenced by the lack of a m/z 944 fragment

ion. Only a very minor fraction of $(dCG\text{-}GAAA(tet\text{-}N_2)K + H)^+$ underwent dissociation to the components, as documented by the very weak peak of $(GAAA(tet\text{-}N_2)K + H)^+$ at m/z 637 (Figure 7b). The spectra can be unequivocally interpreted as evidence for highly efficient and selective nitrile imine cross-linking to the guanine ring. BOMD + DFT calculations of $(dCG\text{-}GAAA(tet)K + H)^+$ precursor complexes indicated low-energy structures in which cytosine was protonated at N-3, and the guanine ring was wedged in a loop formed by GAAA(tet)K (Figure 7a, inset). We note that protonation of free dCG favors the guanine N-7 position, 60 so

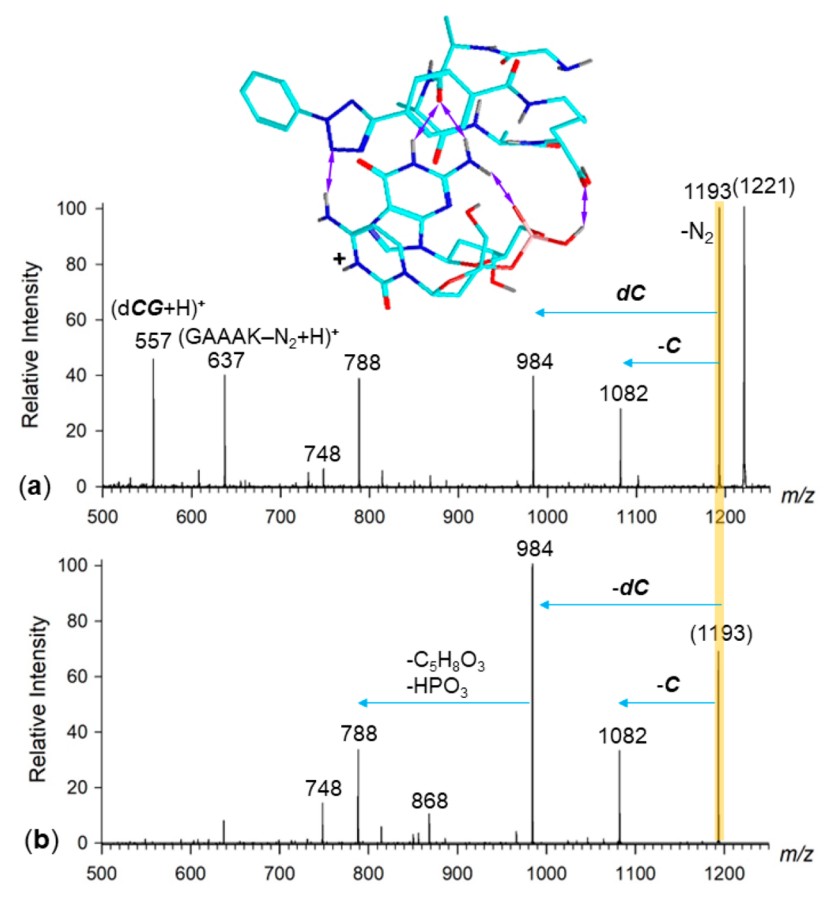


Figure 7. (a) UVPD-MS² spectrum of the (dCG-GAAA(tet)K + H)⁺ complex. Inset shows the M06-2X/6-31+G(d,p)-optimized structure of a low-energy complex ion. Only exchangeable hydrogens are shown to avoid clutter. (b) CID-MS³ spectrum of (dCG-GAAA(tet-N₂)K + H)⁺. Atom color coding is as in Figure 3. Hydrogen bonds are visualized by double-headed purple arrows.

the low energy of cytosine-protonated (dCG-GAAA(tet)K + H)⁺ must be due to the nucleobase coordination to the tetrazole system. This complex geometry may favor proton transfer to the nitrile imine, followed by addition to the guanine ring. The guanine bonds engaged in the nitrile-imine reaction (C=O, N7–C8, etc.), structures of the cross-link(s), and the mechanism of this new reaction are currently being investigated.

CONCLUSIONS

Nitrile imine intermediates that were generated from peptide-2,5-diaryltetrazole conjugates were found to undergo intramolecular cyclizations with peptide amide and carboxyl groups. The generation of the nitrile imine intermediates in conjugates can be done efficiently by CID or UVPD at 250 nm. UVPD is the preferred method for nitrile imine generation in noncovalent ion complexes, which is likely to be the major future application of these novel reactions in gas-phase ions. In particular, the discovered reactivity of peptide amide groups toward nitrile imines appears promising as it provides potential clues to cross-link structure elucidation and conformational analysis. The role of multiple charging, amino acid side-chain functional groups, post-translational modifications, and nucleobases other than guanine in the complexes and their effect on nitrile-imine based cross-linking are the subjects of current research directions in order to explore the applicability of this new method.

ASSOCIATED CONTENT

Supporting Information

The Supporting Information is available free of charge at https://pubs.acs.org/doi/10.1021/jasms.3c00379.

Synthetic procedures, detailed ion mobility parameters, supplementary tables of high-resolution data, tandem mass spectra, and TD-DFT absorption spectra (PDF)

AUTHOR INFORMATION

Corresponding Authors

Karel Lemr — Department of Analytical Chemistry, Faculty of Science, Palacky University, Olomouc 779 00, Czech Republic; Institute of Microbiology of the Czech Academy of Sciences, Prague 142 20, Czech Republic; ⊚ orcid.org/0000-0003-3158-0637; Phone: +420-585 634 415; Email: karel.lemr@upol.cz

František Tureček — Department of Chemistry, Bagley Hall, Box 351700, University of Washington, Seattle, Washington 98195-1700, United States; orcid.org/0000-0001-7321-7858; Phone: +1-206-685-20411; Email: turecek@uw.edu

Authors

Jiahao Wan – Department of Chemistry, Bagley Hall, Box 351700, University of Washington, Seattle, Washington 98195-1700, United States

Marianna Nytka – Department of Analytical Chemistry, Faculty of Science, Palacky University, Olomouc 779 00, Czech Republic Haocheng Qian — Department of Chemistry, Bagley Hall, Box 351700, University of Washington, Seattle, Washington 98195-1700, United States

Kim Vu – Department of Chemistry, Bagley Hall, Box 351700, University of Washington, Seattle, Washington 98195-1700, United States

Complete contact information is available at: https://pubs.acs.org/10.1021/jasms.3c00379

Notes

The authors declare no competing financial interest.

ACKNOWLEDGMENTS

Research at the University of Washington was supported by the Chemistry Division of the U.S. National Science Foundation, grant CHE-1951518. F.T. acknowledges support by the Klaus and Mary Ann Saegebarth Endowment. Research at Palacký University was supported by the project IGA PrF 2023 027.

REFERENCES

- (1) Piersimoni, L.; Kastritis, P. L.; Arlt, C.; Sinz, A. Cross-Linking Mass Spectrometry for Investigating Protein Conformations and Protein—Protein Interactions—A Method for All Seasons. *Chem. Rev.* **2022**, *122*, 7500—7531.
- (2) Shigdel, U. K.; Zhang, J.; He, C. Diazirine-Based DNA Photo-Cross-Linking Probes for the Study of Protein-DNA Interactions. *Angew. Chem., Int. Ed.* **2008**, 47, 90–93.
- (3) Lee, H. S.; Dimla, R. D.; Schultz, P. G. Protein-DNA Photo-Crosslinking with a Genetically Encoded Benzophenone-Containing Amino Acid. *Bioorg. Med. Chem. Lett.* **2009**, *19*, 5222–5224.
- (4) Das, J. Aliphatic Diazirines as Photoaffinity Probes for Proteins: Recent Developments. *Chem. Rev.* **2011**, *111*, 4405–4417.
- (5) Dubinsky, L.; Krom, B. P.; Meijler, M. M. Diazirine Based Photoaffinity Labeling. *Bioorg. Med. Chem.* **2012**, *20*, 554–570.
- (6) Dorman, G.; Prestwich, G. D. Benzophenone Photophores in Biochemistry. *Biochemistry* **1994**, *33*, 5661–5673.
- (7) Shaffer, C. J.; Andrikopoulos, P. C.; Řezáč, J.; Rulíšek, L.; Tureček, F. Efficient Covalent Bond Formation in Gas-Phase Peptide-Peptide Ion Complexes with the Photoleucine Stapler. *J. Am. Soc. Mass Spectrom.* **2016**, *27*, 633–645.
- (8) Nguyen, H. T. H.; Andrikopoulos, P. C.; Rulíšek, L.; Shaffer, C. J.; Tureček, F. Photodissociative Cross Linking of Noncovalent Peptide-Peptide Ion Complexes in the Gas Phase. *J. Am. Soc. Mass Spectrom.* **2018**, *29*, 1706–1720.
- (9) Pepin, R.; Shaffer, C. J.; Tureček, F. Position-Tunable Diazirine Tags for Peptide-Peptide Ion Crosslinking in the Gas-Phase. *J. Mass Spectrom.* **2017**, *52*, 557–560.
- (10) Liu, Y.; Ramey, Z.; Tureček, F. Non-Covalent Interactions of a Neuroprotective Peptide Revealed by Photodissociative Cross-Linking in the Gas Phase. *Chem.-Eur. J.* **2018**, *24*, 9259–9263.
- (11) Huang, S. R.; Liu, Y.; Tureček, F. Non-Covalent Complexes of the Amyloid Peptide Fragment Gly-Asn-Asn-Gln-Gln-Asn-Tyr. A Gas-Phase Photodissociative Cross-Linking and Born-Oppenheimer Molecular Dynamics Binding Study. *Phys. Chem. Chem. Phys.* **2019**, 21, 2046–2056.
- (12) Nguyen, H. T. H.; Huang, S. R.; Liu, Y.; Liu, Y.; Korn, J. A.; Tureček, F. Probing Arginine-Phosphopeptide Interactions in Non-Covalent Peptide-Peptide Ion Complexes Using Gas-Phase Cross-Linking and Born-Oppenheimer Molecular Dynamics Calculations. *Int. J. Mass Spectrom.* **2019**, *435*, 259–271.
- (13) Liu, Y.; Tureček, F. Photodissociative Cross-linking of Diazirine-Tagged Peptides with DNA Dinucleotides. *J. Am. Soc. Mass Spectrom.* **2019**, *30*, 1992–2006.
- (14) Liu, Y.; Liu, Y.; Nytka, M.; Huang, S. R.; Lemr, K.; Tureček, F. Probing D- and L-Adrenaline Binding to β_2 -Adrenoreceptor Peptide

- Motifs by Photodissociation Crosslinking and Ion Mobility Mass Spectrometry. J. Am. Soc. Mass Spectrom. 2021, 32, 1041–1052.
- (15) Tureček, F. Covalent Crosslinking in Gas-Phase Biomolecular Ions. An Account and Perspective. *Phys. Chem. Chem. Phys.* **2023**, 25, 32292–32304.
- (16) Lee, S.; Valentine, S. J.; Reilly, J. P.; Clemmer, D. E. Controlled Formation of Peptide Bonds in the Gas Phase. *J. Am. Chem. Soc.* **2011**, 133, 15834–15837.
- (17) McGee, W. M.; McLuckey, S. A. Efficient and Directed Peptide Bond Formation in the Gas Phase via Ion/Ion Reactions. *Proc. Natl. Acad. Sci. U. S. A.* **2014**, *111*, 1288–1292.
- (18) Cheung See Kit, M.; Webb, I. K. Application of Multiple Length Cross-linkers to the Characterization of Gaseous Protein Structure. *Anal. Chem.* **2022**, *94*, 13301–13310.
- (19) Liu, M. T. H. Chemistry of Diazirines; CRC Press: Boca Raton, FL, 1987; Vols. I and II.
- (20) Frey, H. M.; Stevens, I. D. R. The Photolysis of Dimethyldiazirine. *J. Chem. Soc.* **1963**, 3514–3519.
- (21) Julian, R. R.; May, J. A.; Stoltz, B. M.; Beauchamp, J. E. Biomimetic Approaches to Gas Phase Peptide Chemistry: Combining Selective Binding Motifs with Reactive Carbene Precursors to Form Molecular Mousetraps. *Int. J. Mass Spectrom.* **2003**, 228, 851–864.
- (22) Sharp, J. T. Nitrile Ylides and Nitrile Imines. In Chemistry of Heterocyclic Compounds 59: Synthetic Applications of 1,3-Dipolar Cycloaddition Chemistry Toward Heterocycles and Natural Products; Padwa, A., Pearson, W. H., Eds.; John Wiley & Sons: New York, 2002.
- (23) Shawali, A. S. Reactions of Heterocyclic Compounds with Nitrilimines and Their Precursors. *Chem. Rev.* **1993**, 93, 2731–2777.
- (24) Su, Y.; Zhao, Y.; Chang, B.; Zhao, X.; Zhang, R.; Liu, X.; Huang, D.; Wang, K.-H.; Huo, C.; Hu, Y. [3 + 2] Cycloaddition of para-Quinone Methides with Nitrile Imines: Approach to Spiropyrazoline-cyclohexadienones. *J. Org. Chem.* **2019**, *84*, 6719–6728.
- (25) Voronin, V. V.; Ledovskaya, M. S.; Gordeev, E. G.; Rodygin, K. S.; Ananikov, V. P. [3 + 2]-Cycloaddition of in Situ Generated Nitrile Imines and Acetylene for Assembling of 1,3-Disubstituted Pyrazoles with Quantitative Deuterium Labeling. *J. Org. Chem.* **2018**, *83*, 3819—3828.
- (26) Guo, C.-X.; Zhang, W.-Z.; Zhang, N.; Lu, X.-B. 1,3-Dipolar Cycloaddition of Nitrile Imine with Carbon Dioxide: Access to 1,3,4-Oxadiazole-2(3H)-ones. *J. Org. Chem.* **2017**, *82*, 7637–7642.
- (27) Spiteri, C.; Keeling, S.; Moses, J. E. New Synthesis of 1-Substituted-1H-indazoles via 1,3-Dipolar Cycloaddition of in situ Generated Nitrile Imines and Benzyne. *Org. Lett.* **2010**, *12*, 3368–3371.
- (28) Tu, L.; Gao, L.; Wang, X.; Shi, R.; Ma, R.; Li, J.; Lan, X.; Zheng, Y.; Liu, J. [3 + 2] Cycloaddition of Nitrile Imines with Enamides: An Approach to Functionalized Pyrazolines and Pyrazoles. *J. Org. Chem.* **2021**, *86*, 559–573.
- (29) Fournier-Le Ray, N.; Joly, N.; Fillaut, J. L. Optimising the Synthesis of 2,5-Diaryltetrazoles: The Decisive Choice of the Reaction Solvent. *Tetrahedron* **2023**, *143*, No. 133560.
- (30) Song, W.; Wang, Y.; Qu, J.; Madden, M. M.; Lin, Q. A Photoinducible 1,3-Dipolar Cycloaddition Reaction for Rapid, Selective Modification of Tetrazole-Containing Proteins. *Angew. Chem., Int. Ed. Engl.* **2008**, *47*, 2832–2835.
- (31) Bégué, D.; Qiao, G. G.; Wentrup, C. Nitrile Imines: Matrix Isolation, IR Spectra, Structures, and Rearrangement to Carbodiimides. J. Am. Chem. Soc. 2012, 134, 5339–5350.
- (32) Bégué, D.; Wentrup, C. Carbenic Nitrile Imines: Properties and Reactivity. *J. Org. Chem.* **2014**, *79*, 1418–1426.
- (33) Moriwaki, Y.; Tachikawa, M.; Maeno, Y.; Shimizu, T. Collision Cooling of Ions Stored in Quadrupole Radio-Frequency Trap. *Jpn. J. Appl. Phys.* **1992**, *31*, 1640–1643.
- (34) Pepin, R.; Tureček, F. Kinetic Ion Thermometers for Electron Transfer Dissociation. *J. Phys. Chem. B* **2015**, *119*, 2818–2826.
- (35) Martens, J.; Berden, G.; Gebhardt, C. R.; Oomens, J. Infrared Ion Spectroscopy in a Modified Quadrupole Ion Trap Mass Spectrometer at the FELIX Free Electron Laser Laboratory. *Rev. Sci. Instrum.* **2016**, *87*, 103108/1–103108/8.

- (36) Dang, A.; Korn, J. A.; Gladden, J.; Mozzone, B.; Tureček, F. UV-Vis Photodissociation Action Spectroscopy on Thermo LTQ-XL ETD and Bruker amaZon Ion Trap Mass Spectrometers: A Practical Guide. J. Am. Soc. Mass Spectrom. 2019, 30, 1558–1564.
- (37) Marshall, D. L.; Menzel, J. P.; McKinnon, B. I.; Blinco, J. P.; Trevitt, A. J.; Barner-Kowolik, C.; Blanksby, S. J. Laser Photodissociation Action Spectroscopy for the Wavelength-Dependent Evaluation of Photoligation Reactions. *Anal. Chem.* **2021**, 93, 8091–8098.
- (38) Giles, K.; Ujma, J.; Wildgoose, J.; Pringle, S.; Richardson, K.; Langridge, D.; Green, M. A Cyclic Ion Mobility-Mass Spectrometry System. *Anal. Chem.* **2019**, *91*, 8564–8573.
- (39) Řezáč, J.; Fanfrlik, J.; Salahub, D.; Hobza, P. Semiempirical Quantum Chemical PM6Method Augmented by Dispersion and H Bonding Correction Terms Reliably Describes Various Types of Noncovalent Complexes. J. Chem. Theory Comput. 2009, 5, 1749–1760
- (40) Řezáč, J. Cuby: An Integrative Framework for Computational Chemistry. *J. Comput. Chem.* **2016**, *37*, 1230–1237.
- (41) Berendsen, H. J. C.; Postma, J. P. M.; van Gunsteren, W. F.; DiNola, A.; Haak, J. R. Molecular Dynamics with Coupling to an External Bath. *J. Chem. Phys.* **1984**, *81*, 3684–3690.
- (42) Stewart, J. J. P. MOPAC 16; Stewart Computational Chemistry: Colorado Springs, CO, 2016.
- (43) Becke, A. D. Density-Functional Exchange-Energy Approximation with Correct Asymptotic Behavior. *Phys. Rev. A* **1988**, 38, 3098–3100.
- (44) Grimme, S.; Ehrlich, S.; Goerigk, L. Effect of the Damping Function in Dispersion Corrected Density Functional Theory. *J. Comput. Chem.* **2011**, 32, 1456–1465.
- (45) Nickerson, C. J.; Bryenton, K. R.; Price, A. J. A.; Johnson, E. R. Comparison of Density-Functional Theory Dispersion Corrections for the DES15K Database. *J. Phys. Chem. A* **2023**, *126*, 8712–8722.
- (46) Zhao, Y.; Truhlar, D. G. The M06 Suite of Density Functionals for Main Group Thermochemistry, Thermochemical Kinetics, Noncovalent Interactions, Excited States, and Transition Elements: Two New Functionals and Systematic Testing of Four M06-Class Functionals and 12 Other Functionals. *Theor. Chem. Acc.* 2008, 120, 215–241.
- (47) Singh, U. C.; Kollman, P. A. An Approach to Computing Electrostatic Charges for Molecules. *J. Comput. Chem.* **1984**, *5*, 129–145.
- (48) Besler, B. H.; Merz, K. M., Jr.; Kollman, P. Atomic Charges Derived from Semiempirical Methods. *J. Comput. Chem.* **1990**, *11*, 431–439.
- (49) Ieritano, C.; Crouse, J.; Campbell, J. L.; Hopkins, W. S. A Parallelized Molecular Collision Cross Section Package with Optimized Accuracy and Efficiency. *Analyst* **2019**, *144*, 1660–1670.
- (50) Ieritano, C.; Hopkins, W. S. Assessing Collision Cross Section Calculations Using MobCal-MPI with a Variety of Commonly Used Computational Methods. *Mater. Today Commun.* **2021**, 27, No. 102226.
- (51) Furche, F.; Ahlrichs, R. Adiabatic Time-Dependent Density Functional Methods for Excited State Properties. *J. Chem. Phys.* **2002**, 117, 7433–7447.
- (52) Wigner, E. On the Quantum Correction for Thermodynamic Equilibrium. *Phys. Rev.* **1932**, *40*, 749–759.
- (53) Bonacic-Koutecky, V.; Mitric, R. Theoretical Exploration of Ultrafast Dynamics in Atomic Clusters: Analysis and Control. *Chem. Rev.* **2005**, *105*, 11–66.
- (54) Barbatti, M.; Ruckenbauer, M.; Plasser, F.; Pittner, J.; Granucci, G.; Persico, M.; Lischka, H. Newton-X: A Surface-Hopping Program for Nonadiabatic Molecular Dynamics. Wiley Interdiscip. *Rev. Comput. Mol. Sci.* **2014**, *4*, 26–33.
- (55) Bleiholder, C.; Osburn, S.; Williams, T. D.; Suhai, S.; Van Stipdonk, M.; Harrison, A. G.; Paizs, B. Sequence-Scrambling Fragmentation Pathways of Protonated Peptides. *J. Am. Chem. Soc.* **2008**, *130*, 17774–17789.

- (56) Novak, J.; Lemr, K.; Schug, K. A.; Havliček, V. CycloBranch: De Novo Sequencing of Nonribosomal Peptides from Accurate Product Ion Mass Spectra. *J. Am. Soc. Mass Spectrom.* **2015**, *26*, 1780–1786.
- (57) Zhu, H.; Zima, V.; Ding, E.; Tureček, F. Carbene Crosslinking in Gas-Phase Peptide Ion Scaffolds. *J. Am. Soc. Mass Spectrom.* **2023**, 34, 763–774.
- (58) Vrkic, A. K.; O'Hair, R. A. J.; Foote, S.; Reid, G. E. Fragmentation Reactions of all 64 protonated Trimer Oligonucleotides Via Tandem Mass spectrometry in an Ion Trap. *Int. J. Mass Spectrom.* **2000**, *194*, 145–164.
- (59) Wan, J.; Brož, B.; Liu, Y.; Huang, S. R.; Marek, A.; Tureček, F. Resolution of Identity in Gas-Phase Dissociations of Mono and Diprotonated DNA Codons by ¹⁵N-Labeling and Computational Structure Analysis. *J. Am. Soc. Mass Spectrom.* **2022**, 33, 1936–1950. (60) Liu, Y.; Korn, J. A.; Dang, A.; Turecek, F. Hydrogen-Rich Cation Radicals of DNA Dinucleotides. Generation and Structure
- Elucidation by UV-Vis Action Spectroscopy. J. Phys. Chem. B 2018, 122, 9665–9680.